Supporting information

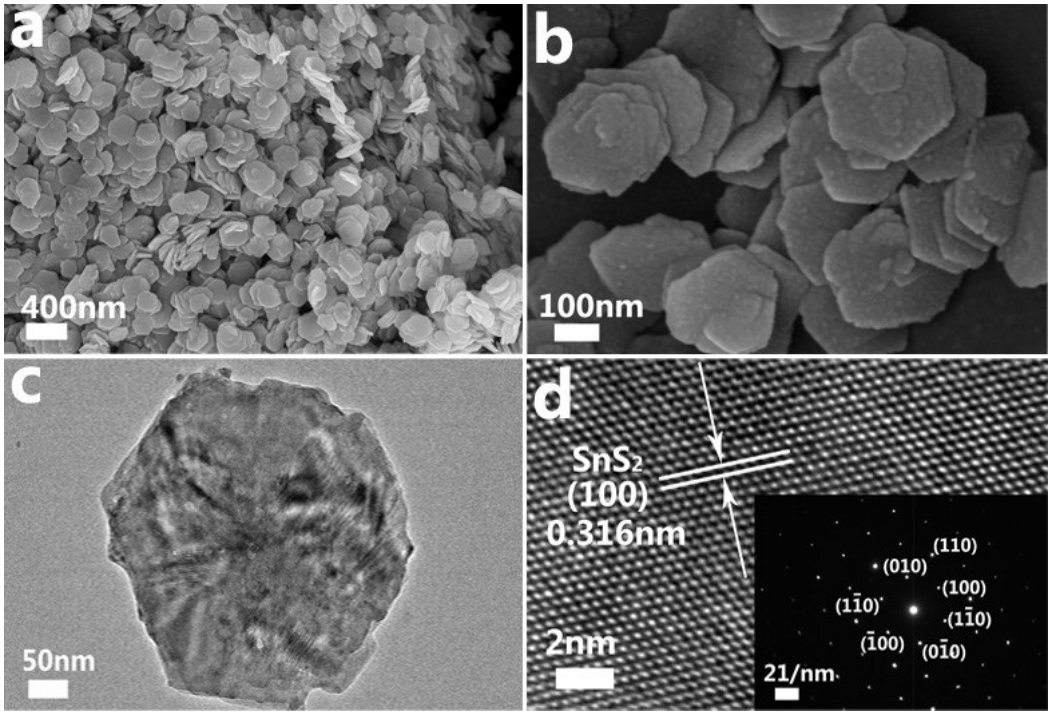

Fig. S1 FESEM images (a, b) and FETEM images (c, d) of as prepared SnS_2 hexagon nanoflakes. Inset in d is the SAED pattern.

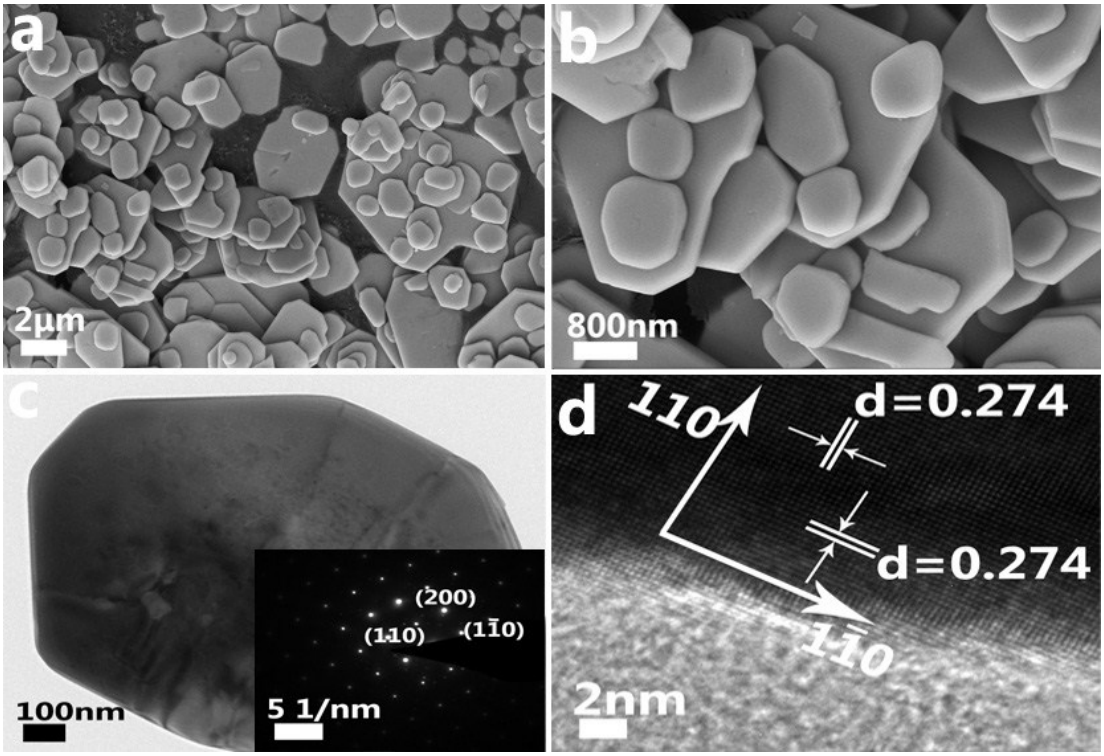

Fig. S2 FESEM images (a, b) and FETEM images (c, d) of as prepared BiOCl nanoflakes. Inset in c is the SAED pattern.

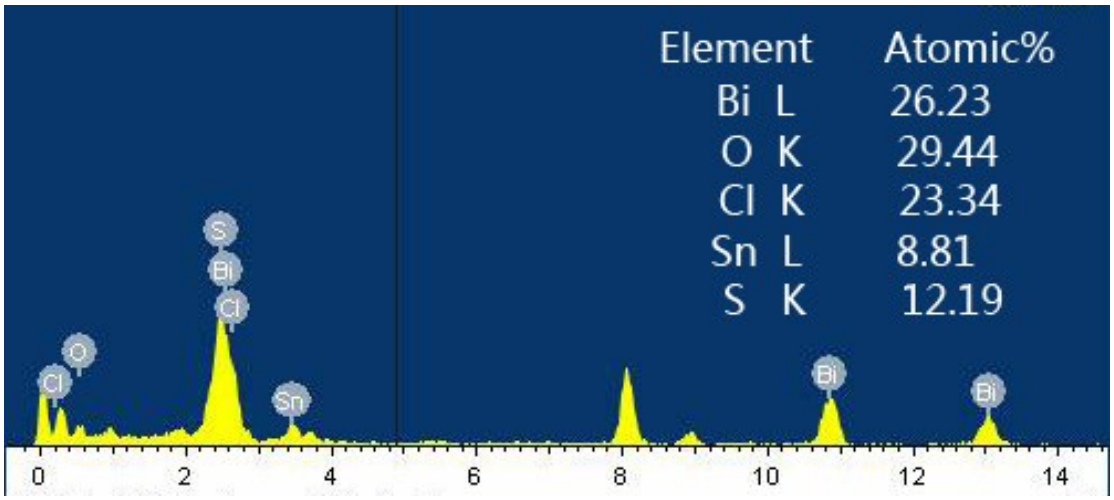

Fig. S3 EDS analysis of the elemental information and atomic percentages of the SnS_2-incorporated BiOCl hollow spheres.

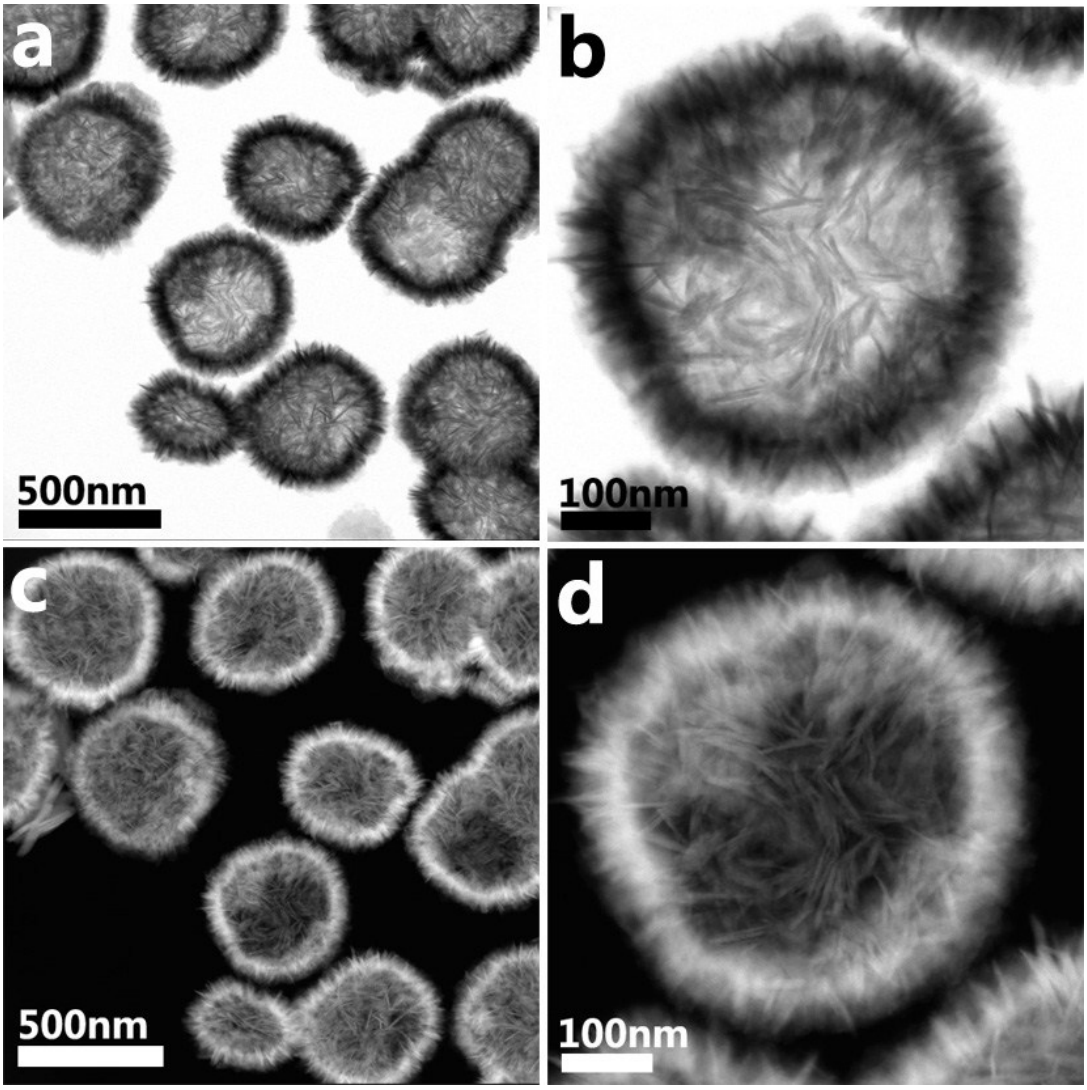

Fig. S4 BF-STEM images (a, b) and HAADF-STEM images (c, d) of SnS_2-incorporated BiOCl hollow spheres.

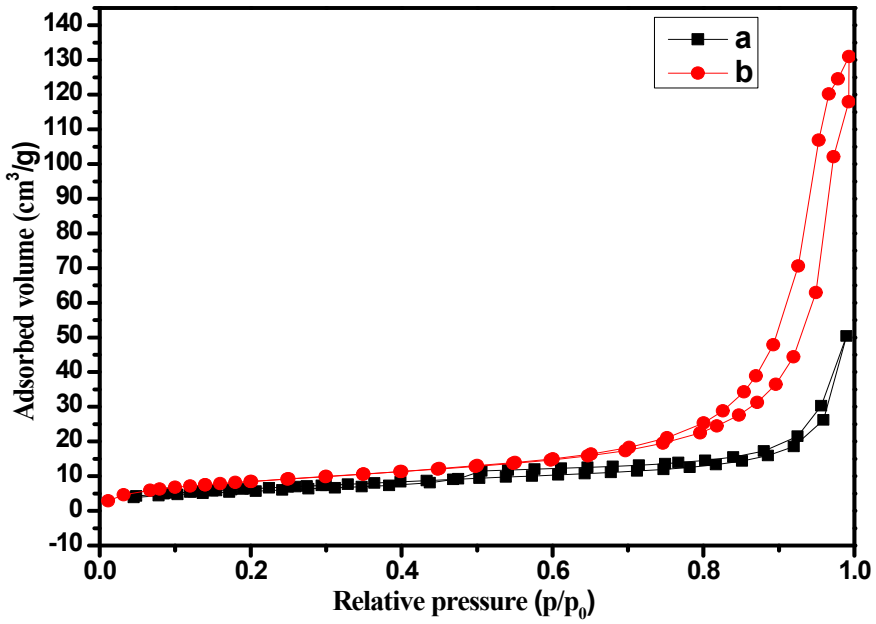

Fig. S5 N_2 adsorption-desorption isotherms and pore-size distribution (inset) of (a) SnS_2-incoporated BiOCl of flower-like structure, (b) SnS_2-incoporated BiOCl hollow spheres.

Table 1 BET properties of SnS_2-incoporated BiOCl samples with different structures.

Samples	A_{BET} (m^2g^{-1})	V_{BJH} (cm^3g^{-1})	Average pore size (Å)
SnS_2-incoporated BiOCl of flower-like structure	23.4383	0.077999	19.39808
SnS_2-incoporated BiOCl hollow spheres	32.5639	0.157919	133.1134

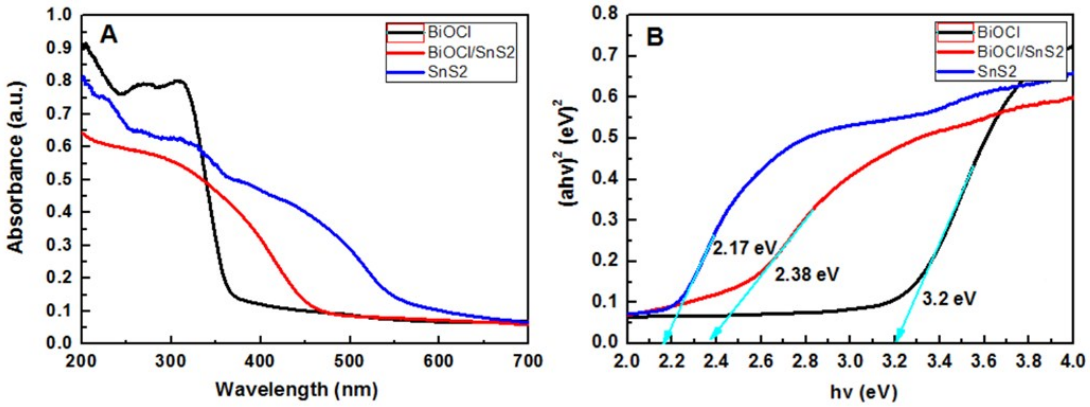

Fig. S6 UV-vis diffuse reflectance spectra (A) and (B) the plot of $(\alpha hv)^{1/2}$ vs band gap energy (hv) of pure SnS_2, pure BiOCl, BiOCl/SnS_2.

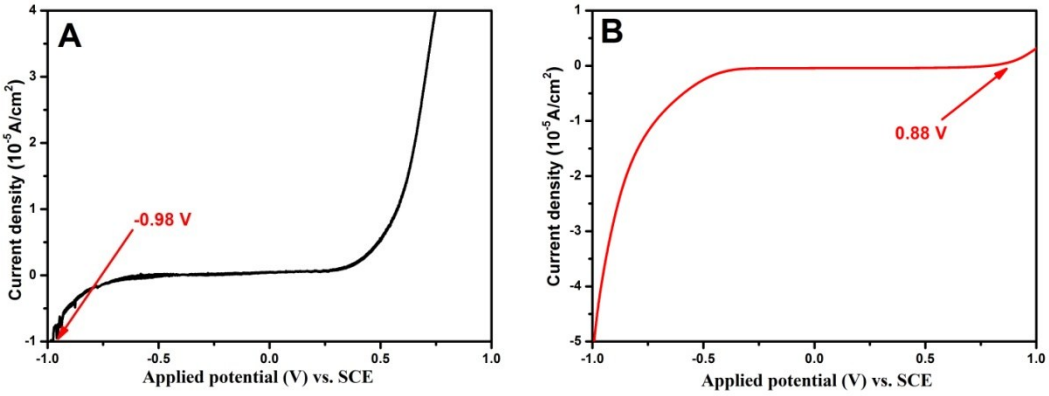

Fig. S7 Current-potential curves for (A) SnS_2 and (B) BiOCl under Xe light irradiation (λ>420 nm).

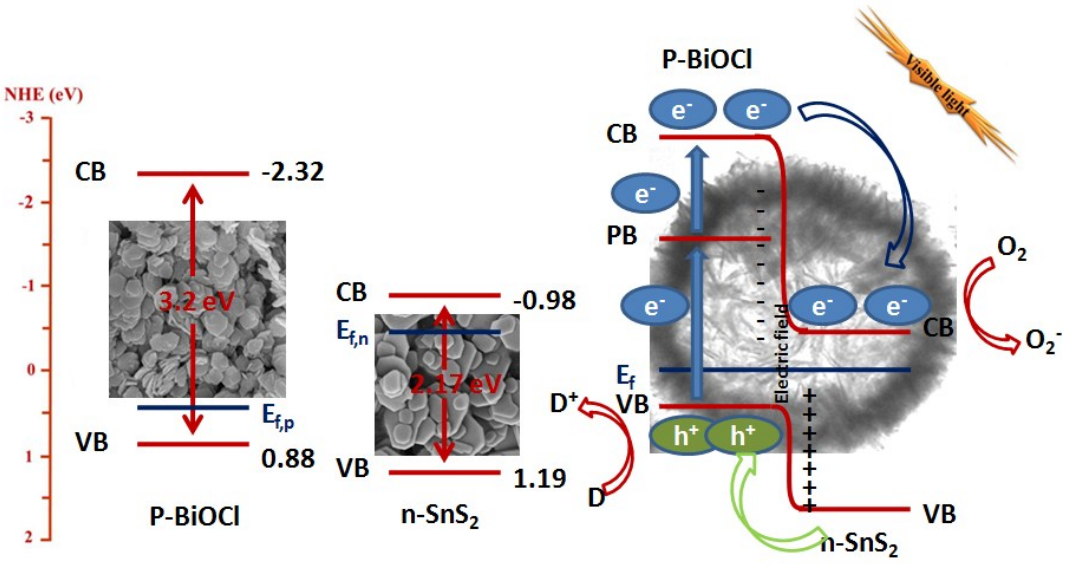

Fig. S8 Schematic diagrams of energy bands of p-BiOCl, n-SnS_2 and the p-BiOCl/n-SnS_2 junction. The energy band diagram at equilibrium and transfer of photoinduced electrons form p-BiOCl and n-SnS_2 under visible-light irradiation are also described.